



Three-dimensional honeycomb-like porous carbon derived from tamarisk roots via a green fabrication process for high-performance supercapacitors

Yingjie Wang¹ · Lianchun Zhao² · Hui Peng¹ · Xiuwen Dai¹ · Xueni Liu¹ · Guofu Ma¹ · Ziqiang Lei¹

Received: 18 February 2019 / Revised: 7 March 2019 / Accepted: 11 March 2019 / Published online: 8 April 2019
© Springer-Verlag GmbH Germany, part of Springer Nature 2019

Abstract

The porous carbon materials derived from biomass have become the most promising candidates for electrochemical energy conversion and storage due to their renewability and sustain ability. Herein, we present a simple activation and carbonization approach to successfully fabricate a novel tamarisk root-based honeycomb-like porous carbon (TRHPC) by using biomass tamarisk roots as carbon precursor and mixed NaCl and ZnCl₂ as hybrid activators. The TRHPC exhibits good electrochemical properties with high specific capacitance 293 F g⁻¹ at a current density of 0.5 A g⁻¹ and high-rate performance (61.4% capacitance retention from 0.5 to 50 A g⁻¹) when it is applied for supercapacitor electrode. Moreover, the symmetric supercapacitor assembled based on the optimized TRHPC electrode materials represents a high energy density of 16 Wh kg⁻¹ at a high power density of 160 W kg⁻¹ and possesses excellent stability with 92% capacitance retention after 10,000 cycles in 0.5 M Na₂SO₄ electrolyte. The excellent electrochemical performance of TRHPC with three-dimensional honeycomb-like porous structure reveals its significance as electrode materials for supercapacitor applications.

Keywords Tamarisk roots · Hybrid activators · Porous materials · Symmetric supercapacitor

Introduction

To face the challenge of the energy depletion and global warming, there is an urgent need for the development of energy

storage devices with high power density and high energy density simultaneously for advanced electronic equipment [1, 2]. Supercapacitor, as a promising candidate for energy storage system, has attracted tremendous attention owing to their high power density, long cycle life, and good reversibility [3–5]. It is well known that the electrode materials are the key to determine the electrochemical performance of supercapacitor, so the development of high-performance electrode materials is essential for the practical use of supercapacitors [6]. Carbon materials have long been recognized as ideal electrode materials for supercapacitors. In recent years, various carbon-based electrode materials have been designed and constructed from the metal-organic frameworks (MOFs) [7–11], polymer spheres [12], polypyrrole [13], and polybenzoxazine-based polymer [14] used as functional material precursors. Unfortunately, the preparation of abovementioned precursor materials more or less unsatisfactory, such as involving tedious procedures, using organic toxic chemicals, time-consuming and expensive, as well as not suitable for scale-up production and practical applications [15–17]. Therefore, selecting low-cost carbon precursors and appropriate preparation methods are great

Yingjie Wang and Lianchun Zhao contributed equally to this work.

Electronic supplementary material The online version of this article (<https://doi.org/10.1007/s11581-019-02966-x>) contains supplementary material, which is available to authorized users.

✉ Hui Peng
penghui@nwnu.edu.cn

✉ Guofu Ma
magf@nwnu.edu.cn

¹ Key Laboratory of Eco-Environment-Related Polymer Materials of Ministry of Education, Key Laboratory of Polymer Materials of Gansu Province, College of Chemistry and Chemical Engineering, Northwest Normal University, Lanzhou 730070, China

² College of Geography and Environment Sciences, Northwest Normal University, Lanzhou 730070, China

significance for prepared advanced high-performance porous carbons with adjustable pore structure parameters and economic advantages in the field of renewable energy research.

Recently, bio-derived activated carbon materials have been widely investigated because of their raw materials abundant and renewable in nature, high electrical conductivity, and excellent chemical stability [18–20]. Some natural biomass materials, such as rice husk [21], catkins [22], bagasse [23], ginkgo leaves [24], pomelo peel [25], waste celtuce leaves [26], and pomegranate husk [27], have been used in production of activated carbons. Among them, three-dimensional (3D) porous biomass-derived carbon materials are currently considered to be the ideal electrode materials [28]. The hierarchical porosity of these carbon materials provides both a conducting pathway for electrons and a fast ion-transport channel [29]. In addition, in order to enhance their electrochemical performance, the various activators are usually used to prepare biomass carbon materials with developed porosity [30, 31]. However, the common acid/base activators, such as KOH and H_3PO_4 , have significant corrosive properties. Besides, the heavy metal salt activator CuCl_2 possesses strong toxicity. Furthermore, the carbon materials activated by these activators usually display a large proportion of narrow microporous characteristics, which limits the transport of large-sized electrolyte ions and weakens the electrochemical performances of carbon-based electrode materials especially at high current densities [32]. Therefore, it is very encouraging to develop mild, low-cost, large-scale, and implementable preparation methods to produce 3D porous carbon with high electrochemical performances [33].

Herein, a novel tamarisk root-based honeycomb-like porous carbon (TRHPC) is successfully prepared by used biomass tamarisk roots as carbon precursor and employed NaCl and ZnCl_2 as hybrid activators. The TRHPC with unique interconnected honeycomb-like morphology and abundant mesopore and micropore structure exhibits the high specific capacitance of 293 F g^{-1} at 0.5 A g^{-1} . In addition, the assembled symmetric supercapacitor based on TRHPC electrodes shows high energy density of 16 Wh kg^{-1} at a high power density of 160 W kg^{-1} and good cycling stability with the capacitance retention rate reached 92% after 10,000 charging/discharging cycles. Therefore, the TRHPC with excellent electrochemical performances has a great potential as promising electrode for supercapacitor applications.

Experimental

Materials

Tamarisk roots were obtained from the Minqin County of China. Zinc chloride (ZnCl_2) and sodium chloride (NaCl)

were purchased from Tianjin Kaitong Chemical Reagent Co., Ltd. All chemical reagents were of analytical grade.

Preparation of TRHPC

Before the experiments, the obtained tamarisk roots were firstly soaked in dilute HCl solution (0.1 M) for 6 h, and then washed with distilled water and freeze-dried for 36 h. After that, the pretreated tamarisk roots (3.0 g) were firstly precarbonized at $550 \text{ }^\circ\text{C}$ for 2 h at a heating rate of $5 \text{ }^\circ\text{C min}^{-1}$ under an atmosphere of N_2 , and the resulting precarbonized tamarisk root product is named as PC-TR.

The TRHPC materials were synthesized as follows: the PC-TR (1.0 g) and ZnCl_2 (2.0 g) were added into the 30 mL NaCl aqueous solutions with different concentrations (1 M, 2 M, and 3 M), followed by magnetic stir for at least 12 h at room temperature. And then, the suspension was further dried in an air-circulating oven at $60 \text{ }^\circ\text{C}$ to form solid precursor mixtures. Subsequently, the obtained precursor mixtures were activated and carbonized at $800 \text{ }^\circ\text{C}$ for 2 h at a heating rate of $5 \text{ }^\circ\text{C min}^{-1}$ under an atmosphere of N_2 . After the sample cooling to room temperature naturally, the resulting products were thoroughly washed with HCl (2 M) to remove inorganic salt, and then, the sample was repeatedly washed by distilled water until neutral pH was reached and dried at $60 \text{ }^\circ\text{C}$ for 24 h. The obtained tamarisk root-based honeycomb-like porous carbon materials were named TRHPC-1, TRHPC-2, and TRHPC-3 based on the used concentrations of NaCl solutions (1 M, 2 M, and 3 M), respectively.

To further explore the influence of NaCl and ZnCl_2 for TRHPC, only 30 mL of 2 M NaCl solution or 2 g ZnCl_2 dissolve in 30 mL distilled water mixed with PC-TR as comparison experiments were also conducted, respectively. The other preparation process is the same as the TRHPC. The obtained samples were named TRHPC-s (only NaCl treatment) and TRHPC-z (only ZnCl treatment), respectively. In addition, the control sample was also prepared by direct carbonation of PC-TR at $800 \text{ }^\circ\text{C}$ for 2 h at a heating rate of $5 \text{ }^\circ\text{C min}^{-1}$ under an atmosphere of N_2 , and the as-obtained sample was named TRHPC-c.

Characterization

The surface morphology of the materials was performed by field emission scanning electron microscopy (FE-SEM, Zeiss). The phase structure was characterized by using an X-ray diffractometer (XRD, D8 ADVANCE) equipped with graphite monochromatized $\text{Cu K}\alpha$ radiation. Raman spectra were collected using an inVia Raman spectrometer (Rainie Salt Public Co. Ltd., Britain) with a laser wavelength of 514 nm. The composite was examined by Brunauer–Emmett–Teller (BET) measurements using the surface area analyzer (77 K, autosorb iQ2).

Electrochemical measurement

In a three-electrode system, the electrochemical measurements were performed at room temperature using a computer-controlled CHI660D electrochemical work station with the Hg/HgO (1 M KOH) as reference electrode, a carbon rod as the counter electrode, and platinum carbon electrode as the working electrode in a 2 M KOH solution, respectively. The working electrode was prepared by mixing the as-prepared materials with commercial conductive carbon black and polymer binder (polyvinylidene fluoride) (80:10:10, mass ratio) in N-methyl-2-pyrrolidone (NMP) solution until it forms a homogeneous slurry. The slurry was coated on nickel foam with a working area of 1.0 cm², and the electrodes were dried at 60 °C for 12 h and then weighted and pressed into sheets under 15 MPa. The total mass of electroactive material was between 3 and 5 mg of each electrode. The electrochemical properties of the electrodes were measured by the cyclic voltammetry (CV), galvanostatic charge–discharge (GCD), and the electrochemical impedance spectroscopy (EIS) tests. The specific capacitance (C_m) value was defined and calculated according to Eq. (1):

$$C_m = \frac{I \times \Delta t}{m \times \Delta v} \quad (1)$$

where I is the discharge current, Δt is the discharge time, Δv represents to the range of charge–discharge voltage, and m is the mass of the active material of the electrode.

For a two-electrode system, the working electrodes were prepared same to the three-electrode system. The two electrodes with identical or very close weight were selected and immersed in 0.5 M Na₂SO₄ electrolytes for 6 h before being assembled into the symmetric supercapacitor configuration. Then, those electrodes fitted with the separator (thin polypropylene film) and 0.5 M Na₂SO₄ electrolyte solution were symmetrically assembled into sandwich-type cell construction (electrode/separator/electrode). The energy density and power density of the symmetric supercapacitor were calculated using Eqs. (2) and (3):

$$E = \frac{1}{7.2} \times C_m \times \Delta v^2 \quad (2)$$

$$P = \frac{E}{\Delta t} \times 3600 \quad (3)$$

where C_m is specific capacitance and Δv is the range of charge–discharge voltage.

Results and discussion

Figure 1 exhibits the preparation process of TRHPC. Firstly, tamarisk roots were performed a simple pretreatment and

precarbonized at 550 °C under N₂ atmosphere. Then, the resulting precarbonized products were mixed with hybrid inorganic salt activators (ZnCl₂ and NaCl) and further one-step activation and high-temperature carbonization to obtain the final TRHPC materials. It is reported that the mixed NaCl solution in carbon precursor can provide high-energy Cl⁻¹ ions to etch the carbon structures and form well-developed micro- and mesoporous structures during high-temperature carbonization process [34]. In addition, the high specific surface area and rich porosity generated in carbon materials can be obtained by the ZnCl₂ activation approach. Therefore, the tamarisk roots mixed with hybrid activators of the ZnCl₂ and NaCl are expected to exploit the novel porous carbon materials with unique morphology and developed porous structure to provide convenient electron/ion transport and diffusion channels for supercapacitor electrode, resulting in excellent electrochemical performance.

The surface morphologies of as-prepared samples were investigated by FE-SEM. The photographs and FE-SEM images of original tamarisk roots and the corresponding carbon materials are shown in Fig. S1. The results show that the microstructure of the tamarisk roots is not destroyed and maintains good structural stability after high-temperature carbonization. Figure 2a–d gives the FE-SEM images of TRHPC-c, TRHPC-z, TRHPC-s, and TRHPC-2, respectively. It is shown that the TRHPC-c material (Fig. 2a) prepared through direct carbonation of PC-TR presents naturally rich porous and a typical 3D honeycomb-like structure consisting of plenty interconnected networks with a diameter from hundreds of nanometers to several microns. The TRHPC-z (Fig. 2b) prepared only by ZnCl₂ treatment displays 3D honeycomb-like structure with some wrinkles in hole wall. The TRHPC-s prepared only by the NaCl treatment shows porous honeycomb-like structure (Fig. 2c), but some hole wall appears to be fractured significantly. As exhibited in Fig. 2d, TRHPC-2 displays the integrated porous honeycomb-like structure with abundant wrinkles in hole wall. The FE-SEM images of other samples (TRHPC-1 and TRHPC-3) prepared similar to TRHPC-2 but different concentrations of NaCl treatment are presented in Fig. S2. Similarly, TRHPC-1 and TRHPC-3 display the integrated porous honeycomb-like structure with some wrinkles in hole wall. The pore size of TRHPC-1 is similar to that of TRHPC-3, while the hole wall of TRHPC-3 is rougher than that of TRHPC-1. Therefore, it can be concluded that the TRHPC with highly crumpled structure in hole wall maintains the interconnected porous honeycomb structure caused by the coactivation of ZnCl₂ and NaCl.

The XRD pattern of the TRHPC-2 in Fig. 3a exhibits two broad peaks around 23.3° and 42.8° corresponding to the (002) and (100) planes of graphite, respectively, demonstrating the formation of typical graphitic carbon structure [35]. By comparison, the weak and broadening peaks are observed in TRHPC-c, revealing the amorphous nature and low

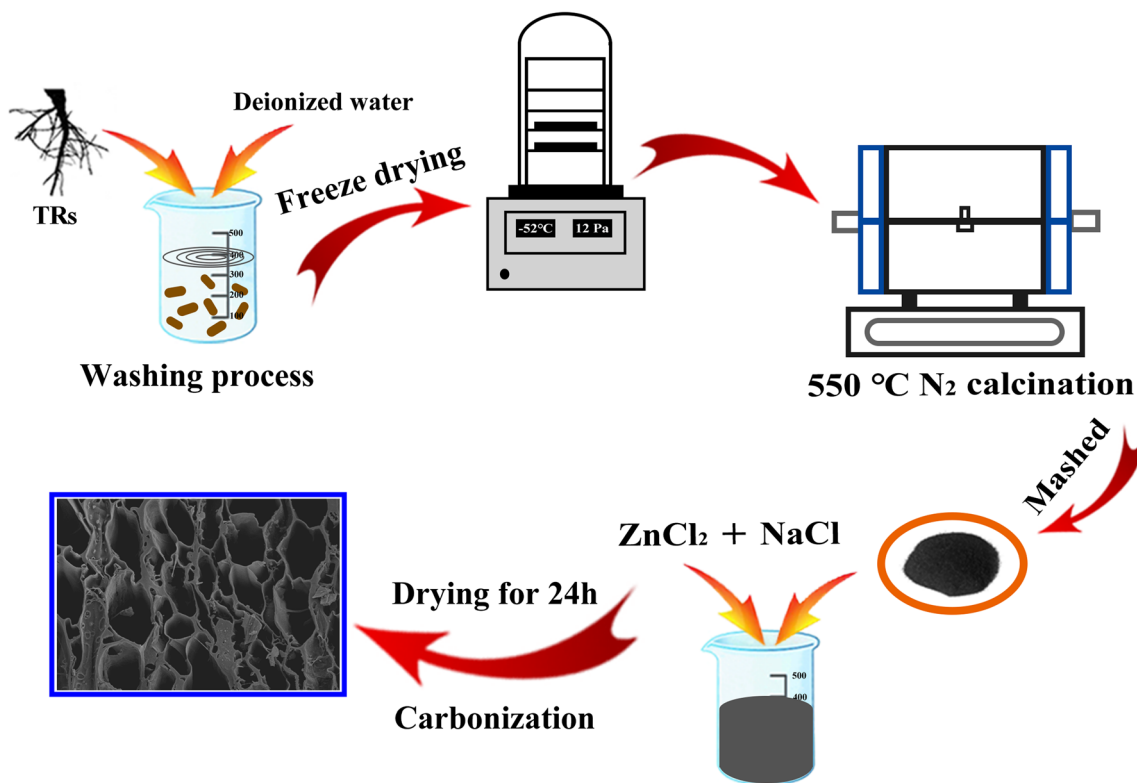
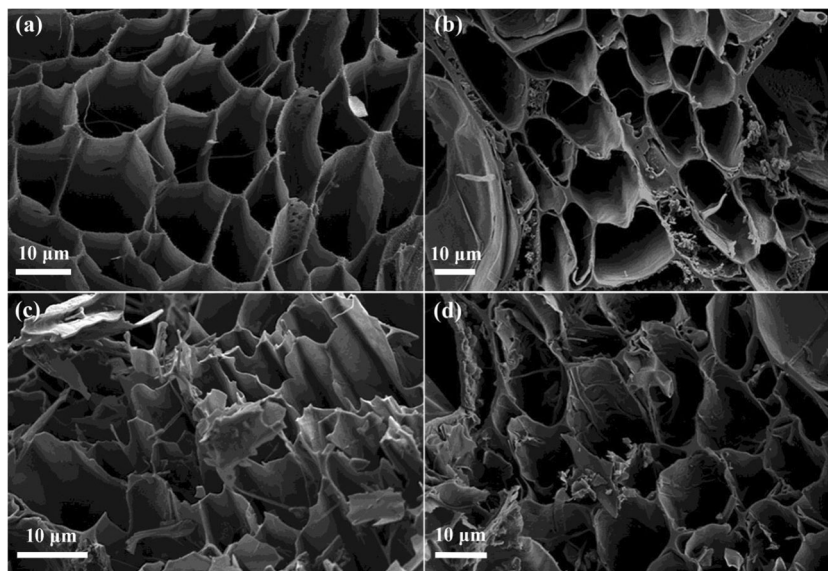


Fig. 1 The schematic illustration of the synthesis of TRHPC

graphitization degree. Figure 3b shows the Raman spectrum of TRHPC-c and TRHPC-2. The two characteristic peaks around 1340 cm^{-1} and 1596 cm^{-1} correspond to the D and G bands of carbon. The D band is a typical characteristic of disordered structure carbon, while the G band is a result of a sp^2 electronic configuration in the graphitic carbon. Therefore, the relative intensity ratio of the D peak to the G peak (I_D/I_G) is commonly used to measure the graphitization degree of carbon materials

[36, 37]. One can calculate that the I_D/I_G ratio of TRHPC-c and TRHPC-2 were 1.03 and 0.96, respectively. The result indicated that the TRHPC-2 possesses a higher graphitization degree and a fewer defective nature compared with TRHPC-c, resulting in high electrical conductivity of TRHPC-2 material. Therefore, it can be concluded that the graphitization degree of carbon materials can be effectively improved by the combination of ZnCl_2 and NaCl activating treatment.

Fig. 2 FE-SEM images of **a** TRHPC-c, **b** TRHPC-z, **c** TRHPC-s, and **d** TRHPC-2



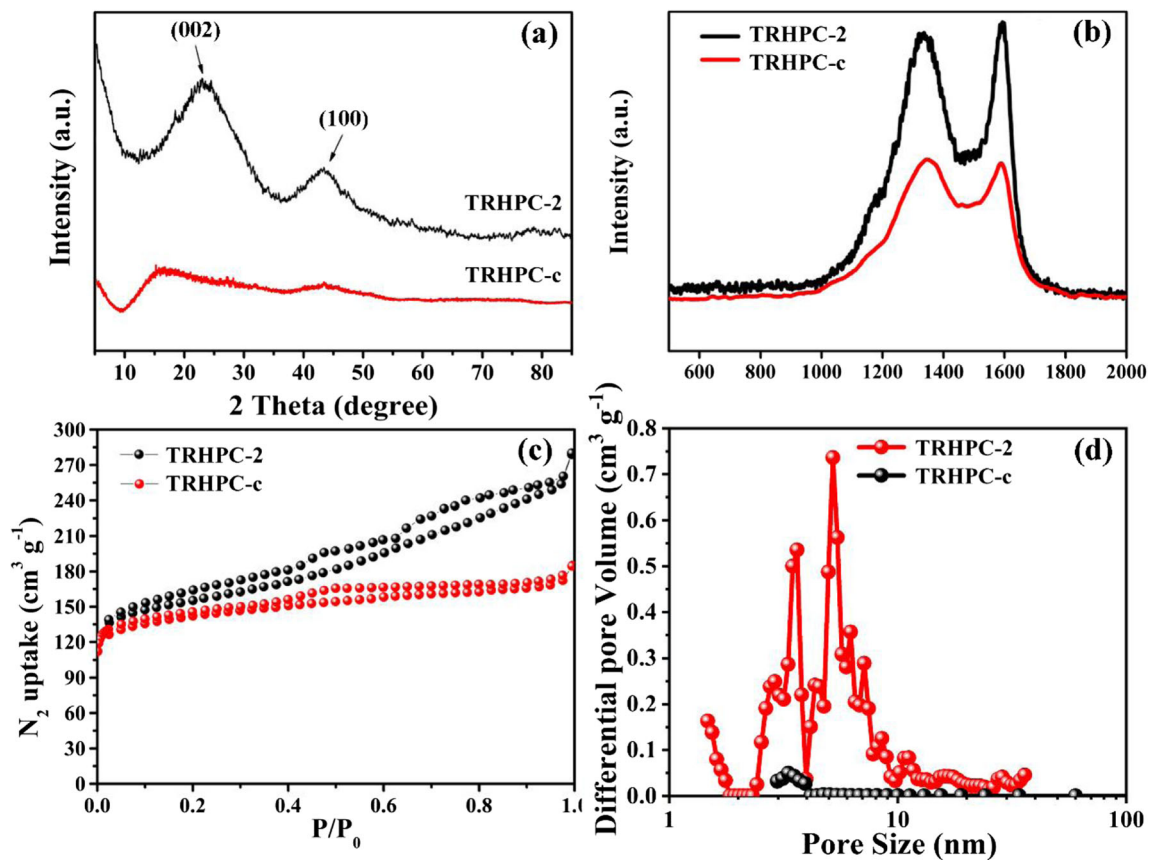


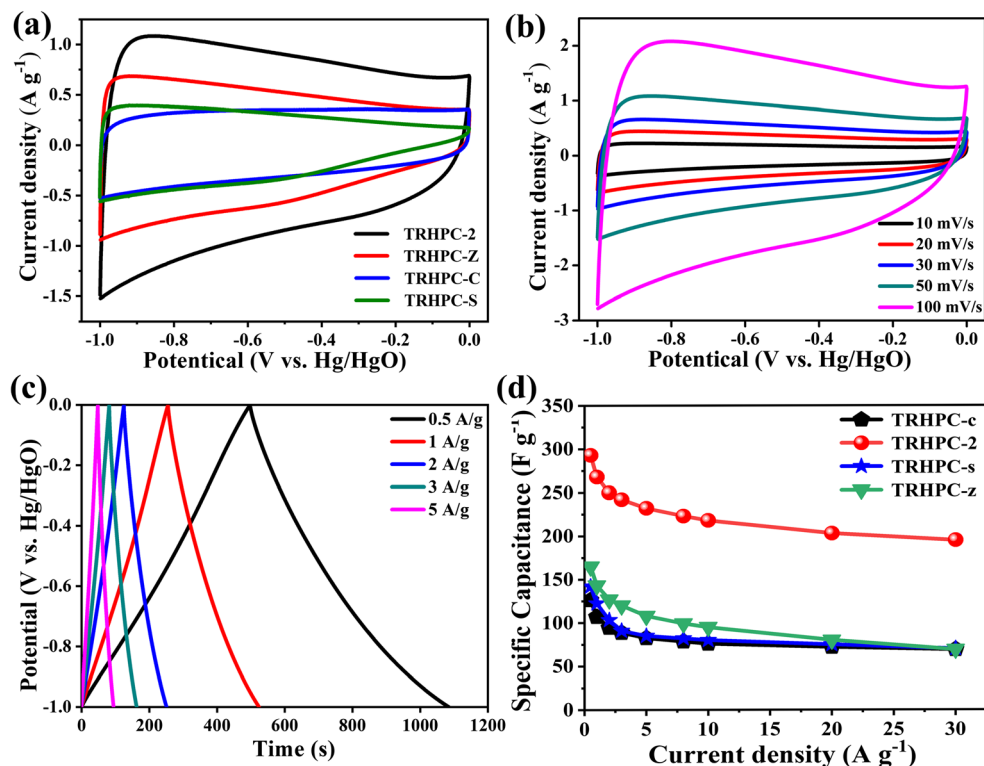
Fig. 3 **a** XRD pattern of TRHPC-c and TRHPC-2. **b** Raman spectrum of TRHPC-c and TRHPC-2. **c** Nitrogen adsorption isotherm. **d** Pore size distribution curves of TRHPC-c and TRHPC-2

It is well accepted that specific surface area and pore structure are two important factors to determine the electrochemical properties of carbon materials. To further study the porosity of TRHPC, the nitrogen adsorption–desorption method was used to determine the BET specific surface area and pore structure of all TRHPC materials. As shown in Fig. 3c, TRHPC-2 and TRHPC-c exhibit typical type IV with a H_3 hysteresis loop, suggesting the existence of mesopore structure of those materials [38, 39]. The amount of adsorbed N_2 at relative high pressures P/P_0 (> 0.90) increase dramatically in the TRHPC-2, demonstrating the presence of large cavities and/or macropore structure [40]. Observably, the adsorbed volume of TRHPC-2 is larger than that of TRHPC-c, meaning large specific surface area and developed pore structure in TRHPC-2. Therefore, it can be concluded that carbonized tamarisk roots integrated by $ZnCl_2$ and $NaCl$ activation can improve porosity and specific surface area of carbon materials. Specifically, the BET specific surface area of TRHPC-2 is $484 \text{ m}^2 \text{ g}^{-1}$, which slightly larger than that of TRHPC-c ($437 \text{ m}^2 \text{ g}^{-1}$). Besides, the corresponding pore-size distribution curves of TRHPC-2 and TRHPC-c calculated by the Barrett–Joyner–Halenda (BJH) method are shown in Fig. 3d. The TRHPC-2 exhibited high

adsorption pore volume and the pore size mainly multi-level distributed in the range of 2–10 nm, while the pore size mainly centered in 12 nm in TRHPC-c. The pore volume of TRHPC-2 is $0.4313 \text{ cm}^3 \text{ g}^{-1}$, which also larger than that of TRHPC-c ($0.2866 \text{ cm}^3 \text{ g}^{-1}$). The existence of large pore volume and abundant small mesopore structure in TRHPC-2 can not only guarantee a large electrode/electrolyte interface for electrostatic charge accumulation but also facilitate ion transport by shortening diffusion pathway, which was beneficial to the performance of the supercapacitor [41].

Electrochemical performances of as-prepared materials were firstly investigated using cyclic voltammetry (CV), galvanostatic charge–discharge (GCD), and electrochemical impedance spectroscopy (EIS) analysis in 2 M KOH electrolyte by a three-electrode system. The CV curve of TRHPC-c, TRHPC-z, TRHPC-s, and TRHPC-2 electrodes were performed at scan rate of 50 mV s^{-1} , as shown in Fig. 4a. Observably, the curve of TRHPC-2 exhibits the rectangular-like shape and larger CV curve area than others, suggesting fast electrochemical response and large specific capacitance of TRHPC-2, which may result from the integrated porous honeycomb structure with abundant wrinkles in hole wall. In contrast, the other materials exhibit small irregular rectangular

Fig. 4 **a** CV curves of TRHPC-2, TRHPC-s, TRHPC-z, and TRHPC-c at scan rate of 50 mV s^{-1} . **b** CV curves of TRHPC-2 at different scan rates. **c** GCD curves of TRHPC-2 at different current densities. **d** Specific capacitance of different electrodes at different current densities



curve and even change to triangular tendency at high potentials, corresponding to low capacitances due to its pore dimensions are probably too small to allow ions to diffuse easily. Remarkably, the CV profiles of TRHPC-2 remain quasi-rectangular shape even when the scan rate increases from 10 to 100 mV s^{-1} (Fig. 4b), indicating the ideal capacitance behavior. The GCD tests of TRHPC-2 were carried out at various current densities ranging from 0.5 to 5 A g^{-1} , as shown in Fig. 4c. The nearly symmetric and linear GCD curves confirm the reversible charging–discharging processes, which are consistent with the CV results. Besides, the comparison of GCD curves of different samples is given in Fig. S3 at a current density of 0.5 A g^{-1} . As shown in Fig. S3, GCD curves of TRHPC-1, TRHPC-2, TRHPC-3, TRHPC-c, TRHPC-s, and TRHPC-z are clearly observed at different current densities of 0.5 to 5 A g^{-1} . Additionally, the specific capacitances of electrode materials calculated from GCD curves at different current densities for all electrodes are shown in Fig. 4d. It can be seen that the specific capacitances of these electrode materials decreased gradually when the current densities increase. The specific capacitance of TRHPC-2 can be reached up to 293 F g^{-1} at 0.5 A g^{-1} , which value is larger than that of TRHPC-c (126 F g^{-1}), TRHPC-z (165 F g^{-1}) and TRHPC-s (142 F g^{-1}) under same current density. It was surprising that the specific capacitance of TRHPC-2 remains 195 F g^{-1} even at a super high current density of 30 A g^{-1} (about 66.6% of the capacitance retention), demonstrating remarkable rate performance. The specific capacitances of TRHPC-1, TRHPC-2,

and TRHPC-3 are shown in Fig. S5. Furthermore, TRHPC-2 displayed capacitance retention of 90.2% after 10,000 cycling operation at current density of 5 A g^{-1} (Fig. S6).

To investigate the practical application of electrode materials, the two-electrode symmetric supercapacitor (SSC) device based on TRHPC-2 electrode was also assembled, and its electrochemical performance was further investigated. It was reported that the neutral aqueous electrolyte (such as Na_2SO_4 and Li_2SO_4) can achieve a higher working voltage than acid or alkali electrolytes, because the neutral electrolyte has a low concentration of hydrogen and hydroxide ions [42]. Therefore, the symmetric supercapacitor based on TRHPC-2 material was fabricated and measured in $0.5 \text{ M Na}_2\text{SO}_4$ electrolyte. As shown in Fig. 5a, the CV curves of as-assembled TRHPC-2//TRHPC-2 SSC were performed at operating voltage of 1.6 V at different scan rates ($10\text{--}50 \text{ mV s}^{-1}$). Moreover, the CV curves of the symmetric supercapacitor can still keep a stable shape even at high scan rate of 50 mV s^{-1} , indicating fast ion transportation and good rate capability. Figure 5b displays the GCD curves of TRHPC-2//TRHPC-2 SSC at different current densities. All GCD curves show approximately the shape of an isosceles triangle, indicating that the device possesses excellent electrochemical reversibility.

The Ragone plot (a plot of energy density vs. power density) of SSC calculated from GCD curves at different current densities is presented in Fig. 5c. It can be found that the energy density of TRHPC-2//TRHPC-2 SSC can be achieved to 16 Wh kg^{-1} at power density of 160 W kg^{-1} and remained

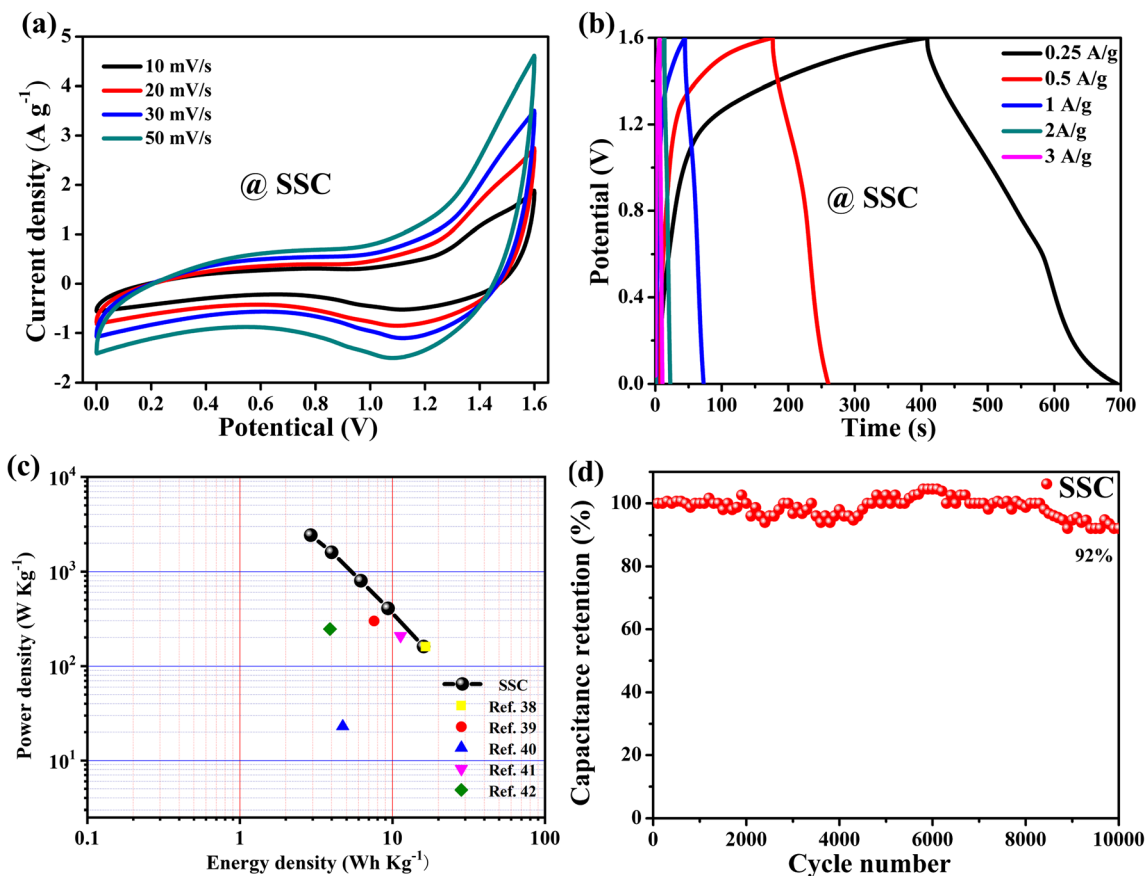


Fig. 5 Electrochemical performance of symmetric supercapacitor measured in a two-electrode system in 0.5 M Na₂SO₄ electrolyte. **a** CV curves of symmetric supercapacitor at different scan rates. **b** GCD curves

of symmetric supercapacitor at various current densities. **c** Ragone plot of the symmetric supercapacitor. **d** Cycling performance of symmetric supercapacitor at a current density of 5 A g⁻¹

as 2.92 Wh kg⁻¹ at 2430 W kg⁻¹, which value is much higher than those of previously reported carbon-based aqueous symmetric supercapacitor [43–47]. Figure S7 shows the Nyquist plots and equivalent circuit diagram of the symmetric supercapacitor. The device shows a small x-axis intercept and vertical line in the high-frequency and low-frequency regions, respectively, indicating a small diffusion resistance and an ideal capacitive behavior. The EIS data were fitted with ZSimp software to the equivalent circuit model (inset in Fig. S7). R_s, R_{ct}, C_{dl}, Z_W, Q, and C_L represent the internal series resistance, charge transfer resistance, electrochemical double-layer capacitance, Warburg impedance, constant phase element, and inductance capacitance, respectively. In terms of the EIS results, the TRHPC-2//TRHPC-2SSC has the low internal resistance (R_s) of 1.65 Ω and low charge transfer resistance (R_{ct}) of 1.39 Ω. Moreover, the TRHPC-2//TRHPC-2 SSC exhibits an outstanding long-term electrochemical stability with 92% of the maximum capacitance remains after 10,000 cycles (Fig. 5d). The remarkable cycling stability can be attributed to the unique 3D honeycomb-like porous structure, which can accelerate diffusion/transport and alleviate the volume changes during the charge–discharge process to guarantee good stability.

Conclusion

In summary, we demonstrated a simple and effective route by using tamarisk roots as carbon precursor and mixed NaCl and ZnCl₂ as hybrid activators to achieve the tamarisk root-based honeycomb-like porous carbon (TRHPC). The TRHPC displays the integrated porous honeycomb-like structure with abundant wrinkles in hole wall. Because of its unique structure, the TRHPC used as electrode for supercapacitors shows a high specific capacitance of 293 F g⁻¹ at 0.5 A g⁻¹ and excellent rate performance. Furthermore, a symmetric supercapacitor is assembled based on TRHPC-2 electrodes, delivering a maximum energy density of 16 Whkg⁻¹ at the power density of 160 W kg⁻¹ and remarkable cycling stability with 92% of the initial capacitance retention after 10,000 cycles. Besides, the impressive electrochemical performances are highly comparable or superior to that of recently reported advanced porous carbons and commercially available activated carbons. Most importantly, the present synthesis strategy can avoid the use of corrosive and/or heavy metal salt activated reagents. The proposed novel method is not only cost-effective and environment-friendly but also suitable for large-scale production of porous carbon materials.

Funding This study was supported by the National Science Foundation of China (21664012, 21703173), the program for Changjiang Scholars and Innovative Research Team in University (IRT15R56), and the Innovation Team Basic Scientific Research Project of Gansu Province (1606RJA324).

Compliance with ethical standards

Conflicts of interest The authors declare that they have no conflicts of interest.

References

- Strauss V, Marsh K, Kowal MD, El-Kady M, Kaner RB (2018) A simple route to porous graphene from carbon nanodots for supercapacitor applications. *Adv Mater* 30:1704449
- Yu S, Zhang Y, Lou G, Wu Y, Zhu X, Chen H, Shen Z, Fu S, Bao B, Wu L (2018) Synthesis of NiMn-LDH nanosheet@Ni₃S₂ nanorod hybrid structures for supercapacitor electrode materials with ultra-high specific capacitance. *Sci Rep* 8:5246
- Kannappan S, Yang H, Kaliyappan K, Manian RK, Pandian AS, Lee YS, Jang JH, Lu W (2018) Thiolated-graphene-based supercapacitors with high energy density and stable cycling performance. *Carbon* 134:326–333
- Chen S, Gao W, Chao Y, Ma Y, Zhang Y, Ren N, Chen H, Jin L, Li J, Bai Y (2018) Low temperature preparation of pore structure controllable graphene for high volumetric performance supercapacitors. *Electrochim Acta* 273:181–190
- Qin T, Liu B, Wen Y, Wang Z, Jiang X, Wan Z, Peng S, Cao G, He D (2016) Freestanding flexible graphene foams@polypyrrole@MnO₂ electrodes for high-performance supercapacitors. *J Mater Chem A* 4: 9196–9203
- Ouyang T, Cheng K, Yang F, Zhou L, Zhu K, Ye K, Wang G, Cao D (2017) From biomass with irregular structures to 1D carbon nanobelts: a stripping and cutting strategy to fabricate high performance supercapacitor materials. *J Mater Chem A* 5:14551–14561
- Tang J, Yamauchi Y (2016) Carbon materials: MOF morphologies in control. *Nat Chem* 8:638–639
- Salunkhe RR, Young C, Tang J, Takei T, Ide Y, Kobayashi N, Yamauchi Y (2016) A high-performance supercapacitor cell based on ZIF-8-derived nanoporous carbon using an organic electrolyte. *Chem Commun* 52:4764–4767
- Wang C, Kaneti YV, Bando Y, Lin J, Liu C, Li J, Yamauchi Y (2018) Metal-organic framework-derived one-dimensional porous or hollow carbon-based nanofibers for energy storage and conversion. *Mater Horiz* 5:394–407
- Zhang W, Jiang X, Zhao Y, Carne-Sanchez A, Malgras V, Kim J, Kim JH, Wang S, Liu J, Jiang JS, Yamauchi Y, Hu M (2017) Hollow carbon nanobubbles: monocrystalline MOF nanobubbles and their pyrolysis. *Chem Sci* 8:3538–3546
- Young C, Wang J, Kim J, Sugahara Y, Henzie J, Yamauchi Y (2018) Controlled chemical vapor deposition for synthesis of nanowire arrays of metal-organic frameworks and their thermal conversion to carbon/metal oxide hybrid materials. *Chem Mater* 30:3379–3386
- Kannagi K (2018) Super critically synthesized V₂O₅ spheres based supercapacitors using polymer electrolyte. *Appl Surf Sci* 456:13–18
- Shrestha S, Mustain WE (2010) Properties of nitrogen-functionalized ordered mesoporous carbon prepared using polypyrrole precursor. *J Electrochem Soc* 157:1665–1672
- Thirukumaran P, Atchudan R, Parveen AS, Lee YR, Kim SC (2018) Polybenzoxazine originated N-doped mesoporous carbon ropes as an electrode material for high-performance supercapacitors. *J Alloy Compd* 750:384–391
- Ramakrishnan P, Park SG, Shanmugam S (2015) Three-dimensional hierarchical nitrogen-doped arch and hollow nanocarbons: morphological influences on supercapacitor applications. *J Mater Chem A* 3:16242–16250
- Liu B, Yang M, Yang D, Chen H, Li H (2018) Medulla tetrapanacis-derived O/N co-doped porous carbon materials for efficient oxygen reduction electrocatalysts and high-rate supercapacitors. *Electrochim Acta* 272:88–96
- Yue F, Gao G, Li F, Zheng Y, Hou S (2018) Size-controlled synthesis of urchin-like reduced graphene oxide microspheres with highly packed density by emulsion-assisted in-situ assembly and their supercapacitor performance. *Carbon* 134:112–122
- Wang C, Wu D, Wang H, Gao Z, Xu F, Jiang K (2018) A green and scalable route to yield porous carbon sheets from biomass for supercapacitors with high capacity. *J Mater Chem A* 6:1244–1254
- Sevilla M, Fuertes AB (2014) Direct synthesis of highly porous interconnected carbon nanosheets and their application as high-performance supercapacitors. *ACS Nano* 8:5069–5078
- Long C, Chen X, Jiang L, Zhi L, Fan Z (2015) Porous layer-stacking carbon derived from in-built template in biomass for high volumetric performance supercapacitors. *Nano Energy* 12:141–151
- Ganesan A, Mukherjee R, Raj J, Shaijumon MM (2014) Nanoporous rice husk derived carbon for gas storage and high performance electrochemical energy storage. *J Porous Mater* 21: 839–847
- Wang K, Yan R, Zhao N, Tian X, Li X, Lei S, Song Y, Guo Q, Liu L (2016) Bio-inspired hollow activated carbon microtubes derived from willow catkins for supercapacitors with high volumetric performance. *Mater Lett* 174:249–252
- Reza MT, Yang X, Coronella CJ, Lin H, Hathwaik U, Shintani D, Neupane BP, Miller GC (2015) Hydrothermal carbonization (HTC) and pelletization of two arid land plants bagasse for energy densification. *ACS Sustain Chem Eng* 4:1106–1114
- Hao E, Liu W, Liu S, Zhang Y, Wang H, Chen S, Cheng F, Zhao S, Yang H (2017) Rich sulfur doped porous carbon materials derived from ginkgo leaves for multiple electrochemical energy storage devices. *J Mater Chem A* 5:2204–2214
- Peng H, Ma G, Sun K, Zhang Z, Yang Q, Lei Z (2016) Nitrogen-doped interconnected carbon nanosheets from pomelo mesocarps for high performance supercapacitors. *Electrochim Acta* 190:862–871
- Zhang Z, Otmar M, Delsing ACA, Stevens MJH, Zhao J, Notten PHL, Dorenbos P, Hintzen HT (2012) Photoluminescence properties of Yb²⁺ in CaAlSiN₃ as a novel red-emitting phosphor for white LEDs. *J Mater Chem* 22:23871–23876
- Sun K, Li J, Peng H, Feng E, Ma G, Lei Z (2017) Promising nitrogen-doped porous nanosheets carbon derived from pomegranate husk as advanced electrode materials for supercapacitors. *Ionics* 23:985–996
- Liang Q, Ye L, Huang ZH, Xu Q, Bai Y, Kang F, Yang QH (2014) A honeycomb-like porous carbon derived from pomelo peel for use in high-performance supercapacitors. *Nanoscale* 6:13831–13837
- Qu S, Wan J, Dai C, Jin T, Ma F (2018) Promising as high-performance supercapacitor electrode materials porous carbons derived from biological lotus leaf. *J Alloy Compd* 751:107–116
- Fechler N, Fellingner TP, Antonietti M (2013) “Salt templating”: a simple and sustainable pathway toward highly porous functional carbons from ionic liquids. *Adv Mater* 25:75–79
- Deng X, Zhao B, Zhu L, Shao Z (2015) Molten salt synthesis of nitrogen-doped carbon with hierarchical pore structures for use as high-performance electrodes in supercapacitors. *Carbon* 93:48–58
- Li Z, Xu Z, Tan X, Wang H, Holt CMB, Stephenson T, Olsen BC, Mitlin D (2013) Mesoporous nitrogen-rich carbons derived from

- protein for ultra-high capacity battery anodes and supercapacitors. *Energy Environ Sci* 6:871–878
33. Chen LF, Lu Y, Yu L, Lou XW (2017) Designed formation of hollow particle-based nitrogen-doped carbon nanofibers for high-performance supercapacitors. *Energy Environ Sci* 10:1777–1783
 34. Liu X, Antonietti M (2014) Molten salt activation for synthesis of porous carbon nanostructures and carbon sheets. *Carbon* 69:460–466
 35. Zhang Q, Han K, Li S, Li M, Li J, Ren K (2018) Synthesis of garlic skin-derived 3D hierarchical porous carbon for high-performance supercapacitors. *Nanoscale* 10:2427–2437
 36. Cançado LG, Takai K, Enoki T, Endo M, Kim YA, Mizusaki H, Jorio A, Coelho LN, Magalhães-Paniago R, Pimenta MA (2006) General equation for the determination of the crystallite size L_a of nanographite by Raman spectroscopy. *Appl Phys Lett* 88:163106
 37. Gao X, Xing W, Zhou J, Wang G, Zhuo S, Liu Z, Xue Q, Yan Z (2014) Superior capacitive performance of active carbons derived from *Enteromorpha prolifera*. *Electrochim Acta* 133:459–466
 38. Yuan C, Zhang X, Su L, Gao B, Shen L (2009) Facile synthesis and self-assembly of hierarchical porous NiO nano/micro spherical superstructures for high performance supercapacitors. *J Mater Chem* 19:5772–5777
 39. Chen X, Zhang J, Zhang B, Dong S, Guo X, Mu X, Fei B (2017) A novel hierarchical porous nitrogen-doped carbon derived from bamboo shoot for high performance supercapacitor. *Sci Rep* 7:7362
 40. Peng H, Ma G, Sun K, Mu J, Lei Z (2014) One-step preparation of ultrathin nitrogen-doped carbon nanosheets with ultrahigh pore volume for high-performance supercapacitors. *J Mater Chem A* 2: 17297–17301
 41. Li X, Liu L, Wang X, Ok YS, Elliott JAW, Chang SX, Chung HJ (2017) Flexible and self-healing aqueous supercapacitors for low temperature applications: polyampholyte gel electrolytes with bio-char electrodes. *Sci Rep* 7:1685
 42. Peng H, Ma G, Sun K, Mu J, Zhang Z, Lei Z (2014) Formation of carbon nanosheets via simultaneous activation and catalytic carbonization of macroporous anion-exchange resin for supercapacitors application. *ACS Appl Mater Interfaces* 6:20795–20803
 43. Su XL, Chen JR, Zheng GP, Yang JH, Guan XX, Liu P, Zheng XC (2018) Three-dimensional porous activated carbon derived from loofah sponge biomass for supercapacitor applications. *Appl Surf Sci* 436:327–336
 44. Misnon II, Zain NKM, Jose R (2018) Conversion of oil palm kernel shell biomass to activated carbon for supercapacitor electrode application. *Waste Biomass Valor* 10:1–10
 45. Li M, Xue J (2014) Integrated synthesis of nitrogen-doped mesoporous carbon from melamine resins with superior performance in supercapacitors. *J Phys Chem C* 118:2507–2517
 46. Sankar KV, Selvan RK (2015) Improved electrochemical performances of reduced graphene oxide based supercapacitor using redox additive electrolyte. *Carbon* 90:260–273
 47. Ye Z, Wang F, Jia C, Shao Z (2018) Biomass-based O, N-codoped activated carbon aerogels with ultramicropores for supercapacitors. *J Mater Sci* 53:12374–12387

Publisher's note Springer Nature remains neutral with regard to jurisdictional claims in published maps and institutional affiliations.